

Enhanced properties of poly(ethylene oxide)/cellulose nanofiber biocomposites

Fatemeh Safdari · Pierre J. Carreau  · Marie C. Heuzey · Musa R. Kamal · Mohini M. Sain

Received: 6 July 2016 / Accepted: 15 November 2016 / Published online: 19 November 2016
© Springer Science+Business Media Dordrecht 2016

Abstract Poly(ethylene oxide) (PEO)/cellulose nanofiber (CNF) biocomposites were developed using a simple aqueous solution technique. A PEO/CNF composite was also produced in the molten state to compare different preparations. The effects of nanofibers on different properties of PEO including rheological, thermal, mechanical and optical were investigated. For the sample prepared in the molten state, no change in properties was observed as compared to the neat matrix. On the other hand, for the solution-based samples, scanning electron microscopy revealed good dispersion/distribution of nanofibers in the PEO, which resulted in a significant increase of the rheological properties and also a

notable shear-thinning behavior. A liquid- to solid-like behavior transition along with the observation of apparent yield stress suggested the formation of a strong CNF 3D network. The Young's modulus and tensile strength of PEO with 3 wt% CNFs were enhanced by 49 and 35%, respectively, compared to the neat PEO. The storage modulus of PEO was significantly improved for all tested temperatures in the dynamic mechanical thermal analysis; at room temperature that corresponds to the rubbery region, a 47% enhancement was observed by incorporating 3 wt% nanofibers. Also, PEO/CNF composites demonstrated good optical transmittance, which is generally not the case with many reinforcements. These results show that PEO/CNF biocomposites with good mechanical and optical properties can be fabricated via a simple aqueous solution technique.

F. Safdari · P. J. Carreau (✉) · M. C. Heuzey
Research Center for High Performance Polymer and Composite Systems (CREPEC), Chemical Engineering Department, Polytechnique Montreal, Montreal, QC H3C 3A7, Canada
e-mail: pcarreau@polymtl.ca

M. R. Kamal
CREPEC, Chemical Engineering Department, McGill University, Montreal, QC H3A 2B2, Canada

M. M. Sain
Faculty of Forestry, University of Toronto, Toronto, ON M5S 3B3, Canada

M. M. Sain
Department of Chemical Engineering and Applied Chemistry, University of Toronto, Toronto, ON M5S 3B3, Canada

Keywords Biocomposites · Poly(ethylene oxide) (PEO) · Cellulose nanofibers (CNFs) · Rheology · Crystallinity · Mechanical properties · Transparency

Introduction

Cellulose nanofibers (CNFs) as a potential reinforcing agent show interesting physical and mechanical properties and exhibit many advantages, which make them preferable over inorganic reinforcements (Azizi Samir

et al. 2004b, 2005a; Frenot et al. 2007; Kloser and Gray 2010; Alloin et al. 2011; Zhou et al. 2011; Miao and Hamad 2013; Xu et al. 2013; Safdari et al. 2016b). They have attracted considerable interest for applications in the automotive, aircraft, railway, and furniture industries as well as sport items, irrigation systems, electrochemicals, etc. (Azizi Samir et al. 2004b, c, 2005a, b; Miao and Hamad 2013; Safdari et al. 2016b). However, CNFs form very strong particle–particle interactions with notable potential for entanglement and agglomeration since they are long and flexible and form hydrogen bonds. Thus, uniformly dispersing the CNFs within polymer matrices is a challenge (Wang and Sain 2007; Iwatake et al. 2008; Nakagaito et al. 2009; Jonoobi et al. 2010; Tingaut et al. 2010; Xu et al. 2014; Safdari et al. 2016b).

The use of more environmentally friendly materials such as biocomposites has been the subject of many studies since they are biodegradable and biocompatible products comprising components from renewable sources, all or in part. Among different biopolymers, poly(ethylene oxide) (PEO) is a nontoxic, highly hydrophilic, semi-crystalline, thermoplastic polymer (Kaczmarek et al. 2007; Zhou et al. 2011; Miao and Hamad 2013). It has already found applications in the medical and biomedical fields, tissue engineering, energy storage (Brown and Laborie 2007; Kaczmarek et al. 2007; Cai and Kim 2010; Zhou et al. 2011; Xu et al. 2013), and the electrochemical field as electrolyte in lithium polymer cells (Azizi Samir et al. 2004b, c, 2005b; Kaczmarek et al. 2007). It has also been used as hydrogel, dispersant, surfactant, flocculating agent and rheology modifier (Kaczmarek et al. 2007; Siró and Plackett 2010). However, neat PEO exhibits low mechanical and thermal properties and high crystallinity, which makes it unsuitable for many applications. Thermal and mechanical properties of PEO can be improved by incorporating reinforcements while retaining its advantageous properties including high biocompatibility, biodegradability (Brown and Laborie 2007; Kaczmarek et al. 2007; Siró and Plackett 2010) and transparency (Park et al. 1999; Elimat 2014).

In view of the above considerations, CNF-reinforced PEO should be an interesting system due to the biocompatibility and biodegradability of the all both key components and final composites. In some studies, to develop enhanced PEO/CNF composites

electrospinning (Fortunato et al. 2012; Xu et al. 2014), which is a slow method for composite preparation and is aimed at special applications, and solution casting (Brown and Laborie 2007; Xu et al. 2013) have been used. To prepare PEO/CNF composites, Brown and Laborie (2007) incorporated PEO in a culture medium of *acetobacter xylinum* (used for bacterial CNF culture). They reported no change in melting temperature of PEO, and a decrease in the crystalline content (from 67% for PEO to 49% for the composite), in the presence of 15 wt% bacterial CNFs. Xu et al. (2013) prepared PEO/CNF composite films by solution casting. A CNF hydrogel was mixed with a PEO solution, allowing PEO molecules to penetrate in the CNF network. They reported a 4 °C decrease in the melting temperature and also a small decrease in the crystalline content of PEO (from 82 to 79%) by adding 4 wt% CNFs; a 46% improvement in the yield strength and a 31% enhancement in the Young modulus of PEO were also reported. However, the solution-based approach is unlikely to be used commercially, as it requires a further step for solvent evaporation, including the use of toxic solvents for polymers not soluble in water. In this regard, other approaches such as the one described by Iyer et al. (2015) comprising a non-solvent-based processing method, solid-state shear pulverization, can be used. Despite this, it is worth mentioning that there are some solution-based techniques such as in situ polymerization that require the use of organic solvents and are nevertheless used in industry (Hamad and Miao 2014).

In our recent work (Safdari et al. 2016b), solvent-casting was employed to incorporate CNFs into polylactide (PLA) as a widely-used biopolymer to overcome some of its drawbacks, e.g. slow crystallization, low thermal stability and heat resistance, which could successfully improve the properties in different aspects without affecting the transparency of the matrix. A 50% increase in Young's and storage moduli at 25 °C, a 264% enhancement in the storage modulus at 70 °C and a 31% increase in the tensile strength of the matrix were achieved for the composite containing 5 wt% CNFs. Moreover, an increase of 11 °C of the crystallization temperature was achieved with 5 wt% CNFs and the composites showed improved thermal stability over PLA. In the current study, a simple aqueous solution technique was used to prepare enhanced PEO/CNF composites with low nanofiber contents. Since there is a lack of information

on light transparency and the molten-state rheological behavior of CNF-filled composites in the literature, we present novel data regarding the effect of CNFs on these properties of PEO. Moreover, the CNF-reinforced PEO biocomposites were characterized in terms of crystallization, mechanical properties, heat resistance and thermal stability. To the best of our knowledge, such a full characterization of PEO/CNF composites has not been reported in the literature. The results of this study point out the great potential of CNFs to reinforce PEO and, thus, to extend the applications of PEO.

Experimental section

Materials

Poly(ethylene oxide) (PEO) in powder form (Sigma-Aldrich Canada Co., Oakville, ON, Canada) with melting point of 65 °C and a viscosity-average molecular weight of 100,000 g/mol was used as the matrix. An aqueous suspension of cellulose nanofibers (CNFs), several micrometers long and less than 50 nm in diameter, was prepared by Janardhnan and Sain following the methodology described in (Janardhnan and Sain 2011). The concentration of nanofibers in the suspension was 2.3 wt%.

Sample preparation

The desired amount of CNF aqueous suspension was diluted with distilled water and stirred for 1 h at the speed of 600 rpm using a magnetic stirrer. At the same time, a solution of the desired amount of PEO in distilled water was prepared using a magnetic stirrer under the same conditions. Thereafter, the diluted CNF suspension was added to the PEO solution while stirring for 1 h. A similar procedure was followed for the neat PEO sample. Then, a vacuum oven was utilized to dry the mixture for 48 h at 50 °C. The composites containing nanofibers were referred to as PLA/*x*CNF, while *x* represents the fiber wt% according to the overall composite weight. For instance, PEO/1CNF denotes that 1% of the overall composite weight consists of CNFs.

To assess the adequacy of the aqueous solution technique in improving the properties, neat PEO and a composite sample containing 3 wt% CNFs were also

prepared in melt via an internal batch mixer, DDRV501 Brabender (C. W. Brabender Instruments Inc., NJ, USA). These samples were coded as PEO (M) and PEO/3CNF (M), respectively, where (M) refers to melt preparation. To do so, the as-received PEO was vacuum dried at 50 °C for 24 h. The aqueous suspension of nanofibers was also freeze-dried in a Labconco Freezone 2.5^{Plus} for 48 h to be directly melt-compounded with PEO at 85 °C and 100 rpm for 7 min under nitrogen atmosphere.

Then, the products of both solution and melt methods were molded in a manual hydraulic press (Carver, Inc., Wabash, IN, USA) at 85 °C for 10 min under a nitrogen atmosphere to produce disks, dumbbells, bars and films for testing. Thereafter, cooling of the samples was done using the press for 5 min at room temperature. The samples were kept under vacuum until characterization.

Characterization

Microscopy

Gold-coated cryo-fractured surfaces of samples were observed by scanning electron microscopy (SEM) using a JEOL JSM 7600TFE instrument (JEOL USA, Inc., Peabody, MA, USA) with an operating voltage of 2 kV.

Rheology

Rheology tests were performed on sample disks of 25 mm diameter and 1 mm thickness, using a stress-controlled Anton Paar MCR 301 rheometer (Anton Paar, Austria). The experiments were conducted at 85 °C in the presence of nitrogen to prevent degradation of the samples. A cone-and-plate geometry with a plate diameter of 25 mm, a cone truncation of 0.051 mm and cone angle of ca. 2° was used to perform measurements in the linear viscoelastic region in the small amplitude oscillatory shear mode. Frequency sweeps were carried out for 85 min at a strain amplitude of 0.05. Prior to the frequency sweep tests, time sweeps were conducted for 85 min at a frequency of 1 rad/s to verify the thermal stability; all the rheological properties of the samples were stable, with increases less than 7%.

Mechanical and thermal properties

Differential scanning calorimetry (DSC) was performed using a DSC Q1000 (TA Instruments, New Castle, DE, USA) under nitrogen. The samples, typically 10 mg, heated at a rate of 2 °C/min and held at 100 °C for 3 min. Thereafter, they were cooled (2 °C/min) to 20 °C. The characterization was performed twice for each sample.

Tensile tests were performed on specimens (63.5 mm long, 9.5 mm wide and 1.6 mm thick) with dumb-bell shape type V (standard ASTM D638) using an Instron 3365 (Instron, Norwood, MA, USA). The tests were performed at room temperature with a load cell of 500 N and a crosshead speed of 5 mm/min. At least seven specimens per sample were tested.

Dynamic mechanical thermal analysis (DMTA) was carried out using a DMA 2980 analyzer (TA Instruments, New Castle, DE, USA). The specimens, rectangular bars of 1.6 mm thickness, 12.2 mm width and 60.5 mm length, were tested in a dual cantilever bending mode at 1 Hz frequency with 30 μm amplitude and a heating rate of 2 °C/min. The measurements were conducted in the range of -100 – 50 °C with a span length of 35 mm on at least three specimens for each sample.

For thermogravimetric analysis (TGA), a TGA Q500 (TA Instruments, New Castle, DE, USA) was used in high-resolution mode. The samples were heated to 800 °C with a rate of 10 °C/min and a nitrogen flow rate of 60 mL/min. The tests were performed twice on typically 15 mg specimen for each sample.

Optical properties

Optical properties were determined using a LAMBDA 1050 UV/Vis/NIR Spectrophotometer (PerkinElmer, Waltham, MA, USA) with 150 mm InGaAs Int-Sphere. The light transparency of the samples was determined quantitatively by the assessment of the corresponding $30 \times 30 \text{ mm}^2$ films of $145 \pm 18 \mu\text{m}$ thickness and used as a measure of the CNF dispersion quality. The wavelength range of 250–800 nm was tested with a 5 nm bandwidth and the rate of 141 nm/min. The characterization was conducted three times for each sample.

Results and discussion

SEM

SEM micrographs of the CNFs (freeze-dried from a suspension of 0.1 wt% nanofibers in water) and PEO containing 3 wt% CNFs prepared in solution and melt are presented in Fig. 1. A web-like structure comprising single fibers and CNF bundles is illustrated in Fig. 1a. It is worth mentioning that even in the preferred medium to disperse CNFs (i.e. water) (Eichhorn et al. 2010) the presence of fiber entanglements and bundles is evident (Fig. 1a). The SEM micrographs of PEO/3CNF (Figs. 1b and c) show quite a good dispersion/distribution of the nanofibers in the PEO matrix without obvious fiber bundles; however, a very large agglomerate is evident in Fig. 1d for the composite sample prepared in the molten state, i.e. PEO/3CNF (M). Also, the presence of some fiber bundles has been observed in our previous investigation on hydrophobic polymer, PLA, CNF composites (Safdari et al. 2016b). The good dispersion/distribution of the nanofibers within PEO is attributed to the efficient aqueous solution technique utilized in the current study.

Rheology

To verify qualitatively the dispersion/distribution of the nanofibers in the matrix, rheological measurements were performed. Figure 2 illustrates the complex viscosity, η^* , and storage and loss moduli, G' and G'' , as functions of the frequency, ω , for the solution-prepared samples. For the neat PEO, a short plateau followed by a shear-thinning behavior on the plot of η^* versus ω (Fig. 2a), and a low-frequency region with a slope of 1.17 for G' (Fig. 2b) are observed, indicating that the terminal zone was not reached at the lowest frequency. By the incorporation of CNFs, the shear-thinning behavior of the composites becomes more evident, mainly at low frequencies (Fig. 2a). Moreover, G' for the composites becomes less frequency dependent at high loadings (Fig. 2b); a low-frequency slope of 0.11 is obtained for PEO/3CNF. The same trend is observed for G'' (Fig. 2b), while the storage modulus is more sensitive to the presence of CNFs. Also, Fig. 2b shows that G' and G'' for PEO/1CNF cross at a frequency lower than that for PEO. It is interesting that for composites containing higher

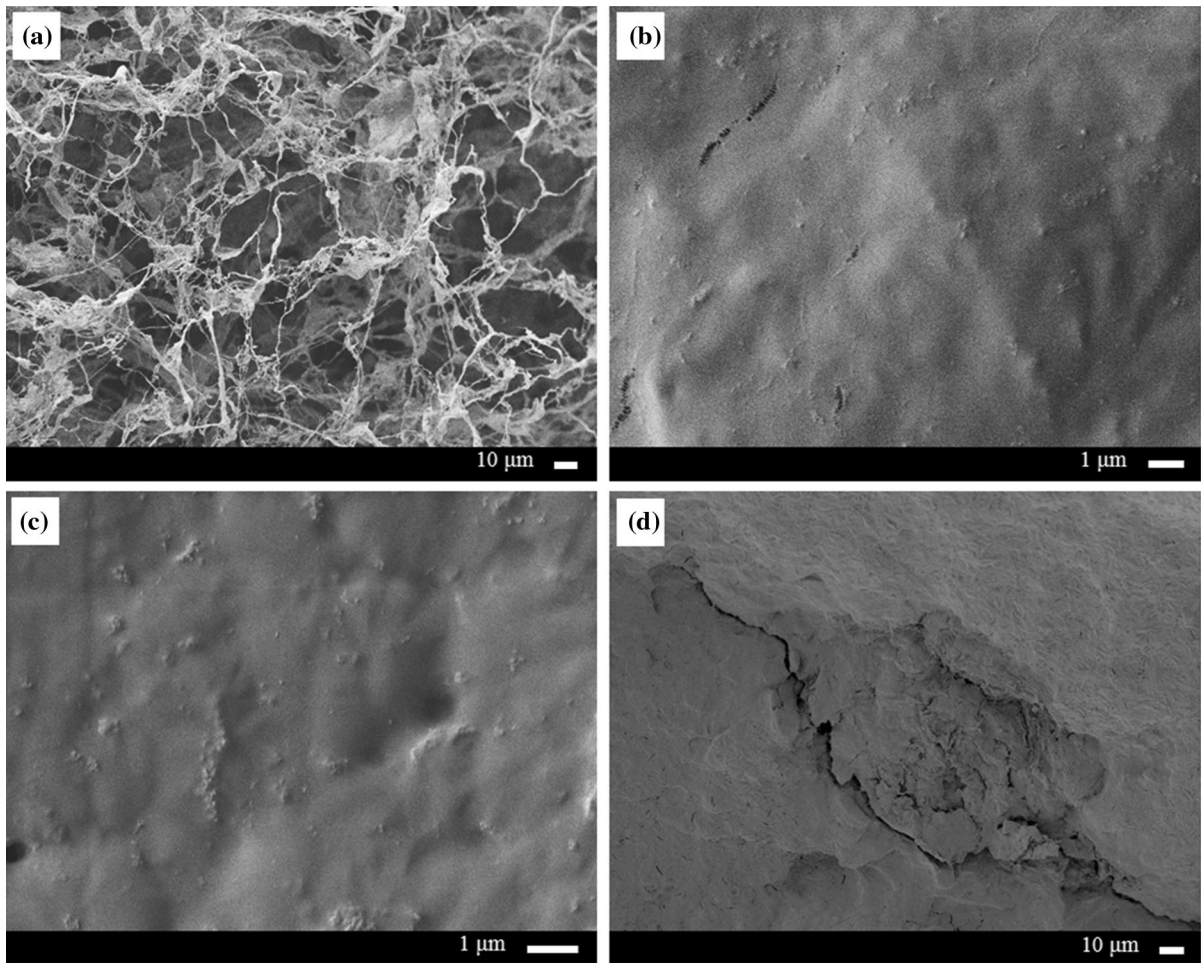


Fig. 1 SEM micrographs of **a** freeze-dried CNFs, **b** and **c** PEO/3CNF for two different samples, and **d** PEO/3CNF (M)

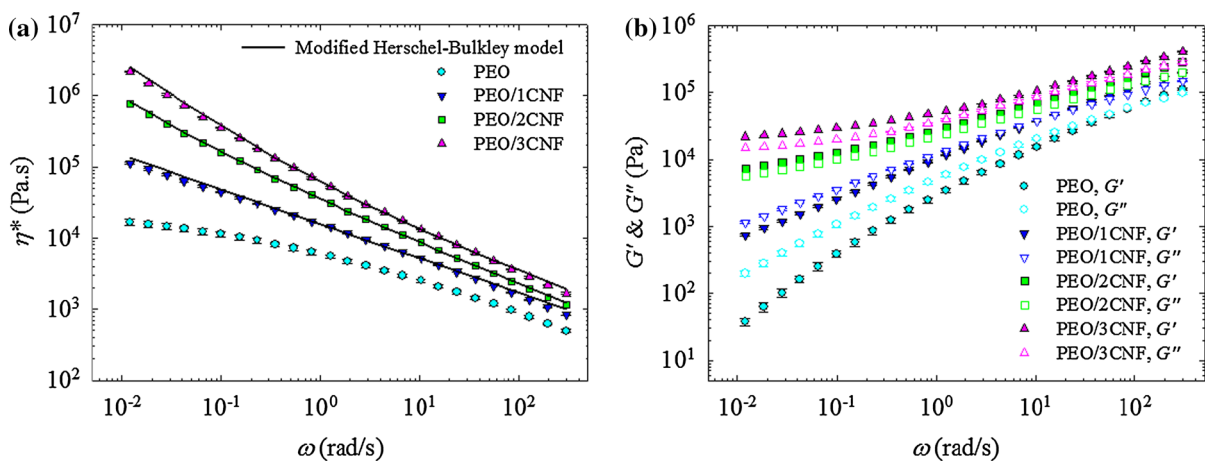


Fig. 2 Plots of **a** complex viscosity, and **b** storage and loss moduli as functions of frequency at 85 °C and strain amplitude of 0.05 for solution-prepared samples. The *solid lines* in **(a)** represent the fits of the modified Herschel–Bulkley model, Eq. (1)

loadings of CNFs, the loss modulus is lower than the storage modulus for the whole range of frequencies tested here. Significant increases up to two, three and two orders of magnitude are observed at low frequencies for η^* , G' and G'' of the composites, respectively, in comparison with the properties of the neat PEO. Likewise, the increases relative to the PLA properties were of two orders of magnitude for η^* , five for G' and two for G'' in the case of the PLA/CNF composite containing 5 wt% nanofibers (Safdari et al. 2016b). These are indicators of a strong nanofiller network along with the interactions between the nanofibers and possibly polymer chains with nanofibers (Hu et al. 2006). Hence, a liquid- to a solid-like behavior transition is observed, with an upturn in viscosity and plateaus at the low-frequency region for G' and G'' along with an apparent yield stress, σ_0 , that can be obtained via the modified Herschel–Bulkley model (Bagheriasl et al. 2016):

$$\eta^* = G_0^*/\omega + k(\gamma^0\omega)^{n-1} \quad (1)$$

and

$$\sigma_0 = G_0^*\gamma^0 \quad (2)$$

where G_0^* is the magnitude of the complex modulus at the lowest frequency, k is a constant, γ^0 is the strain amplitude (0.05) and n is the flow index. The solid lines in Fig. 2a represent the fits of the modified Herschel–Bulkley model. The model is shown to fit very well the data for the composites containing 2 and 3 wt% CNFs with apparent yield stress values of 279 and 1330 Pa, respectively; however, for the composite containing 1 wt% CNFs, due to the lack of good fit at low frequencies, a yield stress of zero was assumed and a good fit could be achieved using the second term of Eq. (1), i.e., $\eta^* = k(\gamma^0\omega)^{n-1}$. As expected, n decreases with the CNF content, from 0.54 for PEO/1CNF to 0.48 for PEO/2CNF and 0.44 for PEO/3CNF. A similar behavior has been observed for other polymer composites such as PLA/CNF (Safdari et al. 2016a, b), PLA/cellulose nanocrystal (CNC) (Kamal and Khoshkava 2015; Bagheriasl et al. 2016), polypropylene/CNC (Khoshkava and Kamal 2014), polyethylene terephthalate/organoclay (Ghanbari et al. 2013a, b) and polycarbonate/carbon nanotube (Abbasi et al. 2009)

It is also believed that the apparent yield stress is observed for concentrations above the rheological

percolation threshold. Here, as the composite samples containing 2 and 3 wt% CNFs exhibit large apparent yield stresses, the percolation is considered to occur at a CNF concentration between 1 and 2 wt%. A percolation concentration in the range of 0.5–1 wt% CNFs and CNCs in a PLA matrix has been previously reported by Safdari et al. (2016b) and Bagheriasl et al. (2016), respectively.

Figure 3 compares η^* and G' as functions of ω , for the matrix and PEO/CNF composites containing 3 wt% CNFs prepared in both solution and melt. PEO and PEO (M) show similar rheological properties. In contrast to the results obtained for the solution-prepared samples, the complex viscosity and storage modulus of PEO/3CNF (M) do not increase compared to those of the neat PEO (M). This emphasizes that dispersing the CNFs even within a polar matrix is quite challenging in direct melt mixing because of the highly entangled structure of the fibers. Hence, the solution technique is better in dispersing the fibers more efficiently in PEO.

DSC

Table 1 presents the results of DSC measurements during the first heating and cooling cycles for various samples. To calculate the crystalline contents, $X_c^{heating}$ and $X_c^{cooling}$, the following equations were used

$$X_c^{heating} = \Delta H_m \times 100 / (w_m \Delta H_m^0) \quad (3)$$

$$X_c^{cooling} = \Delta H_c \times 100 / (w_m \Delta H_m^0) \quad (4)$$

where ΔH_m and ΔH_c are the enthalpies of melting and crystallization, respectively; w_m is the weight fraction of the PEO in each sample and ΔH_m^0 is the melting enthalpy of the 100% crystalline PEO [201.2 J/g (Brown and Laborie 2007)].

The total crystalline content depends on both the number of nuclei and the mobility of polymer chains. By incorporating nanofibers, nucleation would enhance while the polymer chain mobility could be restricted. Here, the overall crystalline content of PEO decreases in both heating and cooling sequences that can be ascribed to the hindrance effect of the CNFs on PEO chain mobility, suppressing their participation into ordered structures that results in smaller and less stable crystals (Brown and Laborie 2007; Zhou et al. 2011). Lowering the large crystalline content of PEO can be beneficial for

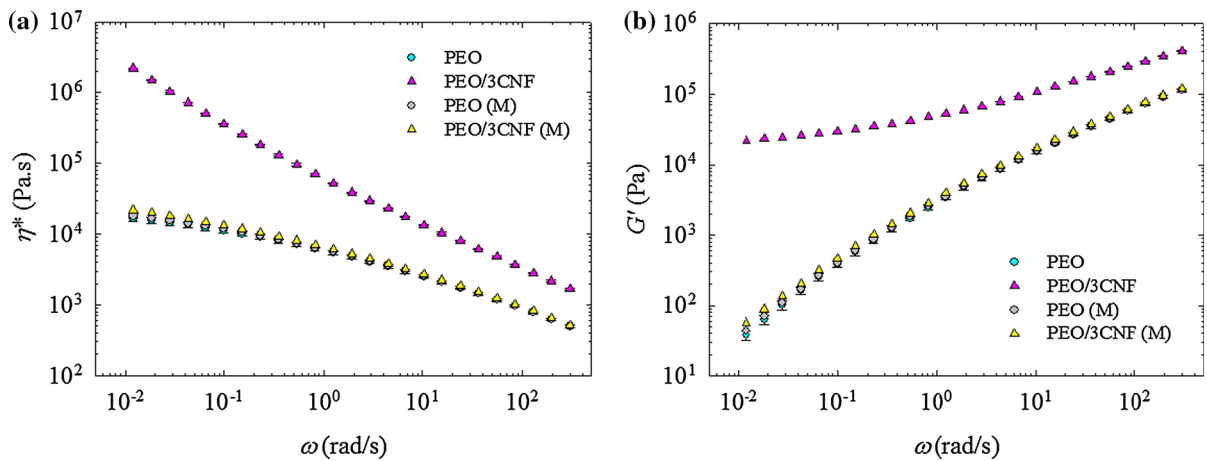


Fig. 3 Plots of **a** complex viscosity and **b** storage modulus as functions of frequency at 85 °C and strain amplitude of 0.05 for PEO and PEO/CNF composites containing 3 wt% CNFs prepared in both solution and melt

Table 1 Results of DSC tests for the first heating and cooling cycles

Sample	T_c (°C)	T_m (°C)	$X_c^{heating}$ (%)	$X_c^{cooling}$ (%)
PEO	50.3 ± 0.1	63.1 ± 0.1	65.4 ± 0.1	65.3 ± 0.1
PEO/1CNF	48.9 ± 0.2	63.0 ± 0.2	61.6 ± 0.1	62.7 ± 0.2
PEO/2CNF	49.8 ± 0.1	63.3 ± 0.1	58.7 ± 0.2	59.2 ± 0.1
PEO/3CNF	49.3 ± 0.2	63.2 ± 0.6	54.6 ± 0.2	55.6 ± 0.3

The data for all temperatures are based on the position of the corresponding peaks

some applications (Azizi Samir et al. 2004b, c, 2005b). Furthermore, the crystallization temperature, T_c , and the melting temperature, T_m , for the composite samples are similar to those of PEO (Table 1). Brown and Laborie (2007) also reported no change in the melting temperature of PEO and a decrease in the crystalline content of PEO (from 67 to 49%) for the sample containing 15 wt% bacterial CNFs. Xu et al. (2013) reported a 4 °C decrease in the melting temperature of PEO and a decrease (from 82 to 79%) in the crystalline content of PEO by incorporating 4 wt% CNFs. Safdari et al. (2016b) also found no change in the melting temperature, up to 11 °C increase in the crystallization temperature and 18% increase in the $X_c^{cooling}$ of the PLA due to the predominance of the nucleating effect of the CNFs for PLA/5CNF.

Tensile properties

Figure 4 reports the normalized Young's modulus, E/E_m , tensile strength, σ/σ_m , and elongation at break,

$\varepsilon/\varepsilon_m$, for all samples (m stands for the matrix, i.e. PEO). For the solution-prepared samples, the Young modulus increases with CNF content (Fig. 4a). For PEO/3CNF the modulus is 1.021 GPa, which corresponds to a 49% increase compared to that of PEO (686.8 MPa). For DSC measurements, the specimens were cut from the samples of tensile tests. Since in the heating sequence the composites show a lower crystallinity compared with the neat PEO (Table 1), their modulus should decrease. However, this negative effect on the modulus of the composites is compensated by the reinforcement effect and/or a strong nanofiber network in the PEO. Figure 4b shows the same trend for tensile strength; an increase of 35% in comparison with PEO (15 MPa) is observed for the solution-prepared composite containing 3 wt% CNFs. This could possibly be ascribed to the enhanced stress transfer from the matrix to the fibers due to a good interaction between the polymer matrix and CNFs (Jonoobi et al. 2010; Miao and Hamad 2013; Safdari et al. 2016b). This strong nanofiber network is also

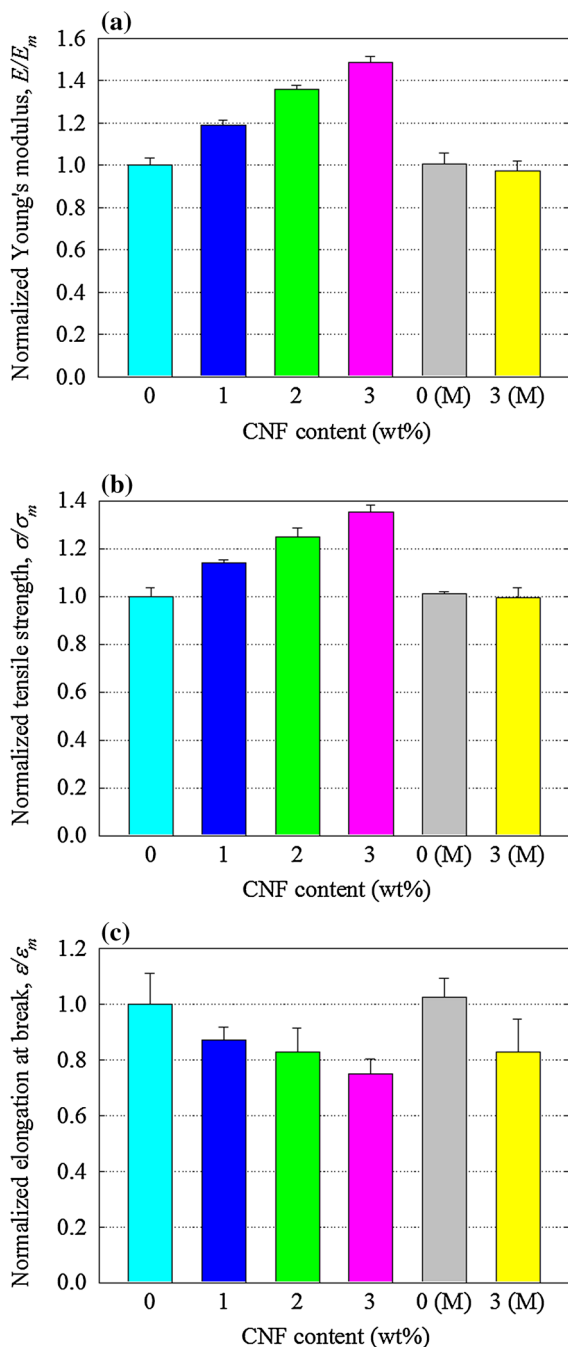


Fig. 4 Normalized **a** Young's modulus, **b** tensile strength, and **c** elongation at break for PEO/CNF samples containing different CNF loadings prepared in both solution and melt. For the neat PEO values of 686.8 MPa, 15 MPa and 6.5% for Young's modulus, tensile strength and elongation at break, respectively, were obtained

advantageous for transferring the load between the fibers (Safdari et al. 2016b). Xu et al. (2013) reported a 31% increase in the Young modulus and 46% increase in the yield strength of PEO by adding 4 wt% CNFs. Safdari et al. (2016b) observed 50 and 31% enhancements in the Young modulus and tensile strength of PLA by adding 5 wt% CNFs. Figure 4c presents the elongation at break for the samples, showing a decrease by ca. 25% for the composite with the largest CNF loading compared with the neat PEO (6.5%). This is the result of reduced chain mobility due to the presence of the filler that generally happens in composite systems (Arias et al. 2013; Safdari et al. 2016b). No enhancement in the Young modulus and tensile strength is observed for the composite sample prepared in the molten state, PEO/3CNF (M), possibly due to the presence of large agglomerates and low content of CNFs. Another probable reason is PEO degradation (reduction of its molecular weight) when the composite was prepared in the molten state at 85 °C and 100 rpm via the internal mixer. Similar results have been reported earlier (Lee et al. 2007; Sanchez-Garcia and Lagaron 2010). As the elongation at break of the neat PEO is already quite low, i.e. 6.5%, the marginally larger value for PEO/3CNF (M) compared to PEO/3CNF cannot provide meaningful information on the relative dispersion of CNFs in these two samples; we also note that the tensile strength values show exactly the reverse trend. Thus, further investigations were only performed on solution-prepared samples.

The Young modulus for fiber-reinforced composites can be predicted using the model developed by Halpin and Kardos (1972). The modulus of a 3D randomly-oriented fiber composite, E , is given by

$$\frac{E}{E_m} = 0.184 \left[\frac{1 + \xi \Psi_L \phi_f}{1 - \Psi_L \phi_f} \right] + 0.816 \left[\frac{1 + 2 \Psi_T \phi_f}{1 - \Psi_T \phi_f} \right] \quad (5)$$

where

$$\Psi_L = (E_f/E_m - 1)/(E_f/E_m + \xi) \quad (6)$$

and

$$\Psi_T = (E_f/E_m - 1)/(E_f/E_m + 2) \quad (7)$$

where E_m and E_f are the Young moduli of the matrix and the fibers, respectively, ϕ_f is the fiber volume fraction, ξ is a shape parameter, which is equal to $0.5l/d$ for high aspect ratio fibers with diameter and length of d and l , respectively (Xu et al. 2013).

To calculate E , the following values were used: $E_m = 686.8$ MPa, $E_f = 150$ GPa (Wang et al. 2006; Safdari et al. 2016b), $\rho_m = 1.13$ g/cm³, $\rho_f = 1.58$ g/cm³ (Wang and Sain 2007; Jonoobi et al. 2010; Safdari et al. 2016b), $d = 50$ nm (Janardhnan and Sain 2011) and l is ca. 20 μ m. Figure 5 compares the experimental data with the predictions of the Halpin–Kardos model for $l/d = 400$, as initially estimated. The model is shown to slightly under-predict the data. Since the nanofibers are highly entangled and form a 3D structure, it is quite hard to estimate the length of the nanofibers. In this regard, a very good fit for the composites of lower CNF contents could be obtained by using a slightly larger aspect ratio, l/d of 553.

DMTA

The storage modulus, E' , and loss tangent, $\tan \delta$ where δ is the phase angle, for the samples over a wide range of temperatures are presented in Fig. 6. The composites show larger values of the storage modulus compared to the neat PEO in both glassy and rubbery regions (Fig. 6a). Moreover, the area under the peak of $\tan \delta$ decreases for the PEO/CNF composites compared to the PEO; the decrease is more important at

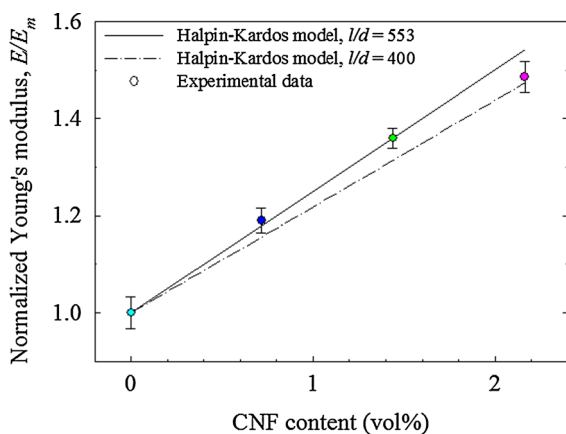


Fig. 5 Predicted values based on the Halpin–Kardos model, Eq. (5) using two aspect ratios for the CNFs, and the experimental data for the normalized Young's modulus of different composite samples

larger CNF loadings. The normalized area, A/A_m , is equal to 0.55 for the highest CNF loading (i.e. 3 wt%). This is an indicator of the reduction of PEO chain mobility due to good dispersion of the fibers (Bagheriasl et al. 2015; Safdari et al. 2016b). A lower decrease in A/A_m , from 1 to 0.62, was reported in our previous study for PLA containing 5 wt% CNFs (Safdari et al. 2016b).

The normalized storage moduli, E'/E'_m , at 20 °C of all samples are compared in Fig. 7. Incorporation of the CNFs into the PEO leads to a significant improvement of the storage modulus due to the good dispersion and reinforcement effect and/or strong entangled network of the cellulosic fibers (Azizi Samir et al. 2004a; Jonoobi et al. 2010; Safdari et al. 2016b). It is worth mentioning that the storage modulus data presents a similar trend as the Young modulus (Fig. 4a). The storage modulus of PEO at 20 °C, 725.2 MPa, increases by 47% for PEO/3CNF (1.064 GPa). Safdari et al. (2016b) reported a 51% increase in storage modulus of PLA at 25 °C for PLA/5CNF.

TGA

Figure 8a illustrates TGA data and Fig. 8b depicts the first derivative of TGA (DTG) for freeze-dried CNFs, PEO and PEO/3CNF. In addition to moisture evaporation (up to 100 °C), PEO and CNF lose 5% of their weight at 380 and 306 °C, respectively, while this temperature is increased to 388 °C for PEO/3CNF. Also, the inflection temperature of PEO increases in the presence of 3 wt% CNFs, while this temperature for CNF is at an even lower temperature. The DTG peak temperature increases for PEO/3CNF compared to the neat PEO (from 384 to 392 °C), while CNF exhibits a peak temperature of 340 °C (Fig. 8b). The degradation for CNF and PEO starts at 317 and 378 °C (onset temperatures), respectively, (Fig. 8b); however, it occurs at 387 °C for PEO/3CNF. The same trend exists for the offset temperature of degradation. Consequently, by the addition of CNFs, the thermal stability of PEO does not deteriorate and slightly improves, as it has been previously reported in other investigations (Safdari et al. 2016b). This can be attributed to restricted polymer chains as a result of the good dispersion and distribution of the

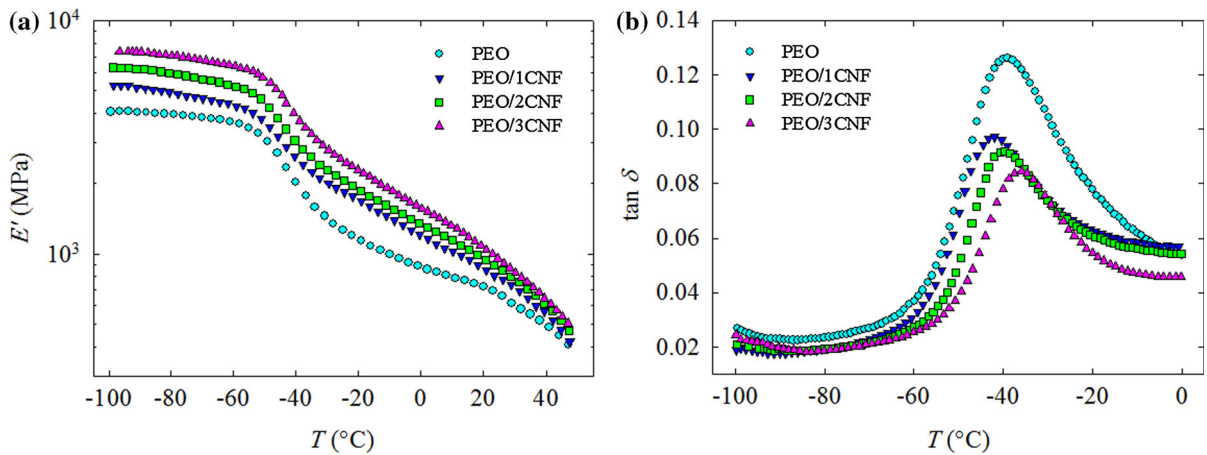


Fig. 6 Plots of **a** storage modulus and **b** $\tan \delta$ of the neat PEO and PEO/CNF composites

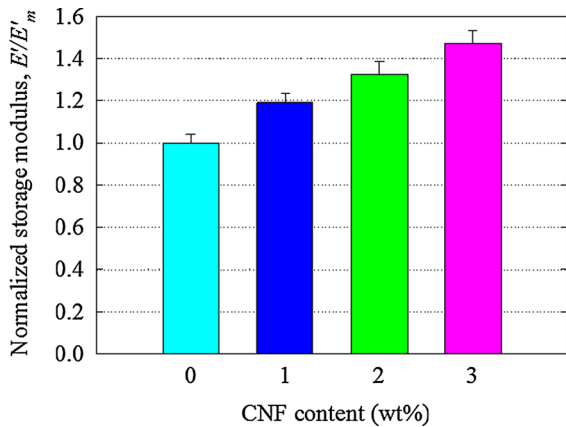


Fig. 7 Normalized values of the storage modulus at 20 °C for various samples. The storage modulus of the neat PEO at 20 °C is 725.2 MPa

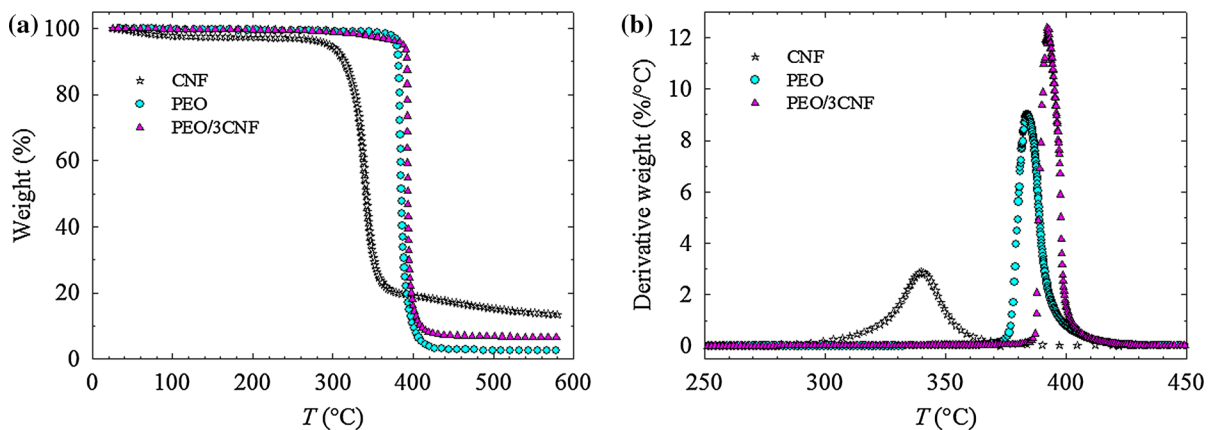


Fig. 8 Plots of **a** TGA and **b** DTG for freeze-dried CNFs, PEO and PEO/3CNF

nanofibers in the PEO (Ramezani Kakroodi et al. 2014; Safdari et al. 2016b).

Optical properties

High transparency of composites for many applications is an asset. A good state of dispersion/distribution of filler in the composite film could help maintaining the original transparency of the neat polymer matrix (Eichhorn et al. 2010; Safdari et al. 2016b). In most cases, films with acceptable transparency should show values greater than 75% in optical transmittance; lower transmittance values correspond to more opaque films (Ambrosio-Martín et al. 2015; Safdari et al. 2016b). The light

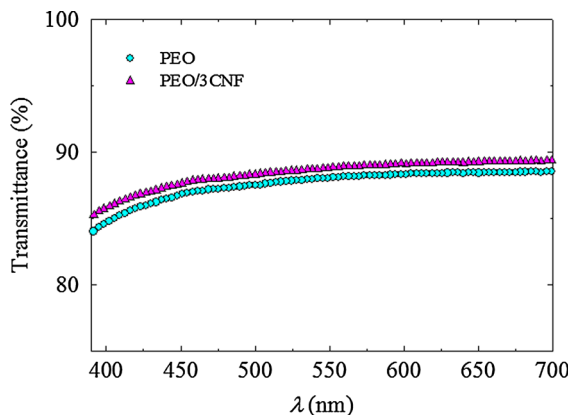


Fig. 9 Light transmittance of PEO and PEO/3CNF films of $145 \pm 18 \mu\text{m}$ thickness

transmittance versus wavelength, λ , is compared in Fig. 9 for the neat PEO and PEO/3CNF films. Over the range of visible light (i.e. $\lambda = 390\text{--}700 \text{ nm}$), the transparencies of both films are quite similar and the addition of CNFs did not compromise the optical properties of PEO, suggesting good dispersion/distribution of CNFs in PEO (Pettersson and Oksman 2006; Safdari et al. 2016b). Moreover, a visual comparison of three different films is presented in Fig. 10. The pictures of PEO and PEO/3CNF films (Figs. 10a and b, respectively) qualitatively show equivalent transparency, whereas for the PEO/3CNF (M) film (Fig. 10c) CNF agglomerates, in the form of white particles, are easily observable on the left side of the picture, indicating inadequate dispersion of nanofibers in this sample. Safdari et al. (2016b) also observed that PLA and PLA/5CNF films show similar transparencies; a decrease of only ca. 5% was reported in transmittance values of PLA film by incorporating 5 wt% CNFs. This provides the opportunity for optical and optoelectronic applications (Siró and Plackett 2010; Janardhnan and Sain 2011; Xu et al. 2013; Kalia et al. 2014; Tercjak et al. 2015; Safdari et al. 2016b), where other reinforcing agents (nanoclays and carbon

nanotubes) deteriorate the transparency of the final products (Xu et al. 2013; Safdari et al. 2016b).

Concluding remarks

A simple aqueous solution technique was used to prepare composites based on PEO and CNFs. The nanofibers were uniformly dispersed within PEO and no large fiber bundles were observed in SEM micrographs. The rheological behavior of the PEO significantly changed in the presence of nanofibers with the percolation threshold being in the range of 1 and 2 wt% CNFs. DSC results confirmed that reinforcing by the CNFs is the main reason for the enhancement of the mechanical properties since the crystalline content of PEO decreased in the presence of nanofibers. The Young modulus and tensile strength of PEO improved for the composites with the CNF content, up to 49 and 35%, respectively, for the composite sample containing only 3 wt% nanofibers. To predict the Young moduli of composites, the Halpin–Kardos model was employed and good agreement between experimental data and the predictions was observed. The storage modulus in DMTA was improved for all tested temperatures and the area under the peak of $\tan \delta$ decreased by incorporating the nanofibers; a 47% enhancement in storage modulus of PEO at $20 \text{ }^\circ\text{C}$ was achieved for PEO/3CNF. Furthermore, considerably larger storage modulus values of the composites compared with the neat PEO were observed at lower temperatures. Moreover, incorporating CNFs enhanced the thermal stability of PEO. The neat PEO and composite films showed similar transparency in the range of visible light.

The composite sample prepared using a melt mixing process did not exhibit any increases in rheological and mechanical properties of the matrix. This shows that dispersing highly entangled CNFs within a polar matrix, such as PEO, is quite challenging and not very easy to achieve via conventional



Fig. 10 Visual comparison of **a** PEO, **b** PEO/3CNF, and **c** PEO/3CNF (M) films (thickness of $145 \pm 18 \mu\text{m}$)

direct melt mixing techniques. Hence, although melt processing is preferable from an industrial point of view, the solution-based preparation method is more efficient to prepare PEO/CNF composites with well-dispersed/distributed structure.

From the results presented in this work, it can be concluded that the reinforcement effect of nanofibers can expand the applications of PEO to cases where good thermal properties, enhanced mechanical properties in a wide temperature range and transparency are important factors. Also, the observed improvements for the PEO/CNF composites compared to PEO point out the importance of the solution technique used in this investigation to finely disperse and distribute CNFs within the PEO matrix.

Acknowledgments The authors are greatly thankful for the financial support from the Natural Sciences and Engineering Research Council of Canada (NSERC) and Network for Innovative Plastic Materials and Manufacturing Processes (NIPMMP). They also appreciated the reviewers' helpful comments.

References

- Abbasi S, Carreau PJ, Derdouri A, Moan M (2009) Rheological properties and percolation in suspensions of multiwalled carbon nanotubes in polycarbonate. *Rheol Acta* 48:943–959. doi:[10.1007/s00397-009-0375-7](https://doi.org/10.1007/s00397-009-0375-7)
- Alloin F, D'Aprea A, Dufresne A, El Kissi N, Bossard F (2011) Poly(oxyethylene) and ramie whiskers based nanocomposites: influence of processing: extrusion and casting/evaporation. *Cellulose* 18:957–973. doi:[10.1007/s10570-011-9543-x](https://doi.org/10.1007/s10570-011-9543-x)
- Ambrosio-Martín J, Fabra MJ, Lopez-Rubio A, Lagaron JM (2015) Melt polycondensation to improve the dispersion of bacterial cellulose into polylactide via melt compounding: enhanced barrier and mechanical properties. *Cellulose* 22:1201–1226. doi:[10.1007/s10570-014-0523-9](https://doi.org/10.1007/s10570-014-0523-9)
- Arias A, Heuzey MC, Huneault M (2013) Thermomechanical and crystallization behavior of polylactide-based flax fiber biocomposites. *Cellulose* 20:439–452. doi:[10.1007/s10570-012-9836-8](https://doi.org/10.1007/s10570-012-9836-8)
- Azizi Samir MAS, Alloin F, Paillet M, Dufresne A (2004a) Tangling effect in fibrillated cellulose reinforced nanocomposites. *Macromolecules* 37:4313–4316. doi:[10.1021/ma035939u](https://doi.org/10.1021/ma035939u)
- Azizi Samir MAS, Alloin F, Sanchez JY, Dufresne A (2004b) Cellulose nanocrystals reinforced poly(oxyethylene). *Polymer* 45:4149–4157. doi:[10.1016/j.polymer.2004.03.094](https://doi.org/10.1016/j.polymer.2004.03.094)
- Azizi Samir MAS, Mateos AM, Alloin F, Sanchez JY, Dufresne A (2004c) Plasticized nanocomposite polymer electrolytes based on poly(oxyethylene) and cellulose whiskers. *Electrochim Acta* 49:4667–4677. doi:[10.1016/j.electacta.2004.05.021](https://doi.org/10.1016/j.electacta.2004.05.021)
- Azizi Samir MAS, Alloin F, Dufresne A (2005a) Review of recent research into cellulosic whiskers, their properties and their application in nanocomposite field. *Biomacromolecules* 6:612–626. doi:[10.1021/bm0493685](https://doi.org/10.1021/bm0493685)
- Azizi Samir MAS, Chazeau L, Alloin F, Cavallé JY, Dufresne A, Sanchez JY (2005b) POE-based nanocomposite polymer electrolytes reinforced with cellulose whiskers. *Electrochim Acta* 50:3897–3903. doi:[10.1016/j.electacta.2005.02.065](https://doi.org/10.1016/j.electacta.2005.02.065)
- Bagheriasl D, Carreau PJ, Dubois C, Riedl B (2015) Properties of polypropylene and polypropylene/poly(ethylene-co-vinyl alcohol) blend/cnc nanocomposites. *Compos Sci Technol* 117:357–363. doi:[10.1016/j.compscitech.2015.07.012](https://doi.org/10.1016/j.compscitech.2015.07.012)
- Bagheriasl D, Carreau PJ, Riedl B, Dubois C, Hamad WY (2016) Shear rheology of polylactide (PLA)–cellulose nanocrystal (CNC) nanocomposites. *Cellulose* 23:1885–1897. doi:[10.1007/s10570-016-0914-1](https://doi.org/10.1007/s10570-016-0914-1)
- Brown EE, Laborie MPG (2007) Bioengineering bacterial cellulose/poly(ethylene oxide) nanocomposites. *Biomacromolecules* 8:3074–3081. doi:[10.1021/bm700448x](https://doi.org/10.1021/bm700448x)
- Cai Z, Kim J (2010) Bacterial cellulose/poly(ethylene glycol) composite: characterization and first evaluation of biocompatibility. *Cellulose* 17:83–91. doi:[10.1007/s10570-009-9362-5](https://doi.org/10.1007/s10570-009-9362-5)
- Eichhorn SJ, Dufresne A, Aranguren M, Marcovich NE, Capadona JR, Rowan SJ, Weder C, Thielemans W, Roman M, Renneckar S, Gindl W, Veigel S, Keckes J, Yano H, Abe K, Nogi M, Nakagaito AN, Mangalam A, Simonsen J, Benight AS, Bismarck A, Berglund LA, Peijs T (2010) Review: current international research into cellulose nanofibres and nanocomposites. *J Mater Sci* 45:1–33. doi:[10.1007/s10853-009-3874-0](https://doi.org/10.1007/s10853-009-3874-0)
- Elimat ZM (2014) Optical characterization of poly(ethylene oxide)/zinc oxide thin films. *Radiat Eff Defect Solids* 169:686–695. doi:[10.1080/10420150.2014.931402](https://doi.org/10.1080/10420150.2014.931402)
- Fortunato G, Zimmermann T, Lübbers J, Bordeanu N, Hufenus R (2012) Reinforcement of polymeric submicrometer-sized fibers by microfibrillated cellulose. *Macromol Mater Eng* 297:576–584. doi:[10.1002/mame.201100408](https://doi.org/10.1002/mame.201100408)
- Frenot A, Henriksson MW, Walkenström P (2007) Electrospinning of cellulose-based nanofibers. *J Appl Polym Sci* 103:1473–1482. doi:[10.1002/app.24912](https://doi.org/10.1002/app.24912)
- Ghanbari A, Heuzey MC, Carreau PJ, Ton-That MT (2013a) Morphological and rheological properties of PET/clay nanocomposites. *Rheol Acta* 52:59–74. doi:[10.1007/s00397-012-0667-1](https://doi.org/10.1007/s00397-012-0667-1)
- Ghanbari A, Heuzey MC, Carreau PJ, Ton-That MT (2013b) A novel approach to control thermal degradation of PET/organoclay nanocomposites and improve clay exfoliation. *Polymer* 54:1361–1369. doi:[10.1016/j.polymer.2012.12.066](https://doi.org/10.1016/j.polymer.2012.12.066)
- Halpin JC, Kardos JL (1972) Moduli of crystalline polymers employing composite theory. *J Appl Phys* 43:2235–2241. doi:[10.1063/1.1661482](https://doi.org/10.1063/1.1661482)
- Hamad WY, Miao C (2014) Nanocomposite biomaterials of nanocrystalline cellulose (NCC) and polylactic acid (PLA). *US* 8,829,110 B2

- Hu G, Zhao C, Zhang S, Yang M, Wang Z (2006) Low percolation thresholds of electrical conductivity and rheology in poly(ethylene terephthalate) through the networks of multi-walled carbon nanotubes. *Polymer* 47:480–488. doi:[10.1016/j.polymer.2005.11.028](https://doi.org/10.1016/j.polymer.2005.11.028)
- Iwatake A, Nogi M, Yano H (2008) Cellulose nanofiber-reinforced polylactic acid. *Compos Sci Technol* 68:2103–2106. doi:[10.1016/j.compscitech.2008.03.006](https://doi.org/10.1016/j.compscitech.2008.03.006)
- Iyer KA, Schueneman GT, Torkelson JM (2015) Cellulose nanocrystal/polyolefin biocomposites prepared by solid-state shear pulverization: superior dispersion leading to synergistic property enhancements. *Polymer* 56:464–475. doi:[10.1016/j.polymer.2014.11.017](https://doi.org/10.1016/j.polymer.2014.11.017)
- Janardhanan S, Sain M (2011) Bio-treatment of natural fibers in isolation of cellulose nanofibres: impact of pre-refining of fibers on bio-treatment efficiency and nanofiber yield. *J Polym Environ* 19:615–621. doi:[10.1007/s10924-011-0312-6](https://doi.org/10.1007/s10924-011-0312-6)
- Jonoobi M, Harun J, Mathew AP, Oksman K (2010) Mechanical properties of cellulose nanofiber (CNF) reinforced polylactic acid (PLA) prepared by twin screw extrusion. *Compos Sci Technol* 70:1742–1747. doi:[10.1016/j.compscitech.2010.07.005](https://doi.org/10.1016/j.compscitech.2010.07.005)
- Kaczmarek H, Bajer K, Gałka P, Kotnowska B (2007) Photodegradation studies of novel biodegradable blends based on poly(ethylene oxide) and pectin. *Polym Degrad Stab* 92:2058–2069. doi:[10.1016/j.polymdegradstab.2007.07.019](https://doi.org/10.1016/j.polymdegradstab.2007.07.019)
- Kalia S, Boufi S, Celli A, Kango S (2014) Nanofibrillated cellulose: surface modification and potential applications. *Colloid Polym Sci* 292:5–31. doi:[10.1007/s00396-013-3112-9](https://doi.org/10.1007/s00396-013-3112-9)
- Kamal MR, Khoshkava V (2015) Effect of cellulose nanocrystals (CNC) on rheological and mechanical properties and crystallization behavior of PLA/CNC nanocomposites. *Carbohydr Polym* 123:105–114. doi:[10.1016/j.carbpol.2015.01.012](https://doi.org/10.1016/j.carbpol.2015.01.012)
- Khoshkava V, Kamal MR (2014) Effect of cellulose nanocrystals (CNC) particle morphology on dispersion and rheological and mechanical properties of polypropylene/CNC nanocomposites. *ACS Appl Mater Interfaces* 6:8146–8157. doi:[10.1021/am500577e](https://doi.org/10.1021/am500577e)
- Kloser E, Gray DG (2010) Surface grafting of cellulose nanocrystals with poly(ethylene oxide) in aqueous media. *Langmuir* 26:13450–13456. doi:[10.1021/la101795s](https://doi.org/10.1021/la101795s)
- Lee JY, Su KE, Chan EP, Zhang Q, Emrick T, Crosby AJ (2007) Impact of surface-modified nanoparticles on glass transition temperature and elastic modulus of polymer thin films. *Macromolecules* 40:7755–7757. doi:[10.1021/ma071332s](https://doi.org/10.1021/ma071332s)
- Miao C, Hamad WY (2013) Cellulose reinforced polymer composites and nanocomposites: a critical review. *Cellulose* 20:2221–2262. doi:[10.1007/s10570-013-0007-3](https://doi.org/10.1007/s10570-013-0007-3)
- Nakagaito AN, Fujimura A, Sakai T, Hama Y, Yano H (2009) Production of microfibrillated cellulose (MFC)-reinforced polylactic acid (PLA) nanocomposites from sheets obtained by a papermaking-like process. *Compos Sci Technol* 69:1293–1297. doi:[10.1016/j.compscitech.2009.03.004](https://doi.org/10.1016/j.compscitech.2009.03.004)
- Park OH, Eo YJ, Choi YK, Bae BS (1999) Preparation and optical properties of silica-poly(ethylene oxide) hybrid materials. *J Solgel Sci Technol* 16:235–241. doi:[10.1023/a:1008717219952](https://doi.org/10.1023/a:1008717219952)
- Petersson L, Oksman K (2006) Biopolymer based nanocomposites: comparing layered silicates and microcrystalline cellulose as nanoreinforcement. *Compos Sci Technol* 66:2187–2196. doi:[10.1016/j.compscitech.2005.12.010](https://doi.org/10.1016/j.compscitech.2005.12.010)
- Ramezani Kakroodi A, Cheng S, Sain M, Asiri A (2014) Mechanical, Thermal, and morphological properties of nanocomposites based on polyvinyl alcohol and cellulose nanofiber from *aloe vera* rind. *J Nanomater* 2014:1–7. doi:[10.1155/2014/903498](https://doi.org/10.1155/2014/903498)
- Safdari F, Bagheriasl D, Carreau PJ, Heuzey MC, Kamal MR (2016a) High-performance polylactide biocomposites reinforced with cellulose nanofibers. *SPE Plast Res Online*. doi:[10.2417/spepro.006650](https://doi.org/10.2417/spepro.006650)
- Safdari F, Bagheriasl D, Carreau PJ, Heuzey MC, Kamal MR (2016b) Rheological, mechanical, and thermal properties of polylactide/cellulose nanofiber biocomposites. *Polym Compos*. doi:[10.1002/pc.24127](https://doi.org/10.1002/pc.24127)
- Sanchez-Garcia M, Lagaron J (2010) On the use of plant cellulose nanowhiskers to enhance the barrier properties of polylactic acid. *Cellulose* 17:987–1004. doi:[10.1007/s10570-010-9430-x](https://doi.org/10.1007/s10570-010-9430-x)
- Siró I, Plackett D (2010) Microfibrillated cellulose and new nanocomposite materials: a review. *Cellulose* 17:459–494. doi:[10.1007/s10570-010-9405-y](https://doi.org/10.1007/s10570-010-9405-y)
- Tercjak A, Gutierrez J, Barud HS, Domenegueti RR, Ribeiro SJL (2015) Nano- and macroscale structural and mechanical properties of in situ synthesized bacterial cellulose/PEO-b-PPO-b-PEO biocomposites. *ACS Appl Mater Interfaces* 7:4142–4150. doi:[10.1021/am508273x](https://doi.org/10.1021/am508273x)
- Tingaut P, Zimmermann T, Lopez-Suevos F (2010) Synthesis and characterization of bionanocomposites with tunable properties from poly(lactic acid) and acetylated microfibrillated cellulose. *Biomacromolecules* 11:454–464. doi:[10.1021/bm901186u](https://doi.org/10.1021/bm901186u)
- Wang B, Sain M (2007) The effect of chemically coated nanofiber reinforcement on biopolymer based nanocomposites. *Bioresources* 2:371–388
- Wang S, Cheng Q, Rials TG, Lee SH (2006) Cellulose microfibril/nanofibril and its nanocomposites. The 8th Pacific rim bio-based composites symposium, Kuala Lumpur, Malaysia, 20–23. Forest Research Institute Malaysia, pp 301–308
- Xu X, Liu F, Jiang L, Zhu JY, Haagenson D, Wiesenborn DP (2013) Cellulose nanocrystals vs. cellulose nanofibrils: a comparative study on their microstructures and effects as polymer reinforcing agents. *ACS Appl Mater Interfaces* 5:2999–3009. doi:[10.1021/am302624t](https://doi.org/10.1021/am302624t)
- Xu X, Wang H, Jiang L, Wang X, Payne SA, Zhu JY, Li R (2014) Comparison between cellulose nanocrystal and cellulose nanofibril reinforced poly(ethylene oxide) nanofibers and their novel shish-kebab-like crystalline structures. *Macromolecules* 47:3409–3416. doi:[10.1021/ma402627j](https://doi.org/10.1021/ma402627j)
- Zhou C, Chu R, Wu R, Wu Q (2011) Electrospun polyethylene oxide/cellulose nanocrystal composite nanofibrous mats with homogeneous and heterogeneous microstructures. *Biomacromolecules* 12:2617–2625. doi:[10.1021/bm200401p](https://doi.org/10.1021/bm200401p)